Effective rheology mapping for characterizing polymer solutions utilizing ultrasonic spinning rheometry

Kohei OHIE[1], Taiki YOSHIDA[2], Yuji TASAKA[1], and Yuichi MURAI[1]

1 Laboratory for Flow Control, Faculty of Engineering, Hokkaido University, N13 W8, 060-8628 Sapporo, Japan

2 National Metrology Institute of Japan, National Institute of Advanced Industrial Science and Technology, Tsukuba Central 3, 1-1-1, Umezono, 305-8563 Tsukuba, Japan

Abstract

We propose a practical map representation termed rheology mapping for comprehensively evaluating the dependence of viscoelasticity on applied shear deformation and shear timescale represented by oscillation frequency, utilizing ultrasonic spinning rheometry (USR), which has excellent applicability to a wide variety of polymer solutions. The rheology mapping was applied to two typical kinds of polymer solutions. One is carboxymethyl cellulose (CMC) aqueous solution, a well-known viscous and shear thinning fluid. The other is polyacrylamide (PAM) aqueous solution generally considered as a viscoelastic fluid while its viscoelasticity is difficult to be evaluated by a standard torque-type rheometer. The rheology mapping for the solutions showed notable rheological properties. The viscoelasticity of both the CMC and PAM solutions vary widely from elastic to viscous, depending on the applied shear rate, strain, and oscillation frequency. The mapping also revealed the clear dependence of the viscosity of the solutions: the CMC solutions on the shear rate and the PAM solutions on the shear strain. These results provide quantitative support of findings in other reports associating these macroscopic properties with the microscopic dynamics of polymer coils.

Corresponding author
Yuji Tasaka (e-mail: tasaka@eng.hokudai.ac.jp)

1 Introduction

Evaluating the rheology of polymer solutions is essential for applying functions of the solutions in material development, quality control of products, and optimal design of production lines. Polymer solutions exhibit various properties such as viscoelasticity, shear thinning/thickening characteristics, and yield stress. These macroscopic properties are exhibited since microstructures, which are uniquely formed based on chemical conditions such as the type of the solved polymer, its molecular weight, and concentration, change depending on both the degree of applied shear deformation and shear timescale represented by oscillation frequency.

A thorough and informative discussion of the dependence of viscoelasticity on the shear strain and frequency was originally given by Pipkin (1986), classifying fluid properties into three characteristics: viscous, viscoelastic, and elastic. According to this concept, the variations in viscoelasticity can be displayed in a two-dimensional diagram representing Deborah and Weissenberg numbers (Reiner 1964; Phan-Thien and May-Duy 2017). This diagram is utilized for qualitative evaluations in arranging Lissajous curves (Hyun et al. 2011), measured by a standard torque-type rheometer (Ewoldt et al. 2007, 2017). By quantitatively characterizing the shape of the Lissajous curves, it was succeeded to quantitatively map both the shear strain and frequency dependence in viscoelasticity (Ewoldt et al. 2008). Although the quantitative map representation is extremely useful for characterizing polymer solutions and motivating development of optimal rheology models for numerical simulations (Larson and Desai 2015), its range of application is still limited to specific polymer solutions showing ideal deformation/flow characteristics in the measurements of a standard rheometer.

The standard rheometer assumes a constant shear rate in the narrow gap filled with test fluids and indirectly evaluate the rheological properties by measuring rotation speed and axial torque. Previous studies however have so far suggested that entangled network structures in polymer solutions would induce elastic instability, shear history, shear banding, and wall-slip phenomena in the measurements of standard rheometers (Fischer et al. 2002; Sui and McKenna 2007; Fardin et al. 2014). These cause spatial variations of shear rate in the narrow gap of the rheometer. Under these specific conditions, the conventional torque-type rheometer cannot distinguish whether the evaluated viscoelasticity is originated by unique properties of polymer solutions themselves or just superimposed phenomenon by the shear banding and wall-slip. Measurements conducted under the heterogeneous conditions cause bias errors in the determinations of the viscoelasticity (de Souza Mendes et al. 2014; Saint-Michel et al. 2016). Previous research therefore utilized the standard rheometer in combination with velocity profiling for determining the actual shear deformation under undesired deformation/flow conditions (Gallot et al. 2013; Fardin et al. 2014; Shiratori et al. 2016). Through those developments, it has been confirmed that geometries of standard rheometers with narrow gaps would be a factor in

the problems. Based on this, we have recently developed a rheometry with a simple open cylindrical vessel, termed ultrasonic spinning rheometry (USR) (Shiratori et al. 2013; Tasaka et al. 2015; Yoshida et al. 2017; Tasaka et al. 2018). The basic concept of the USR is to solve the equations of motion as rheological properties by substituting velocity profiles obtained by ultrasonic velocity profiler (UVP) (Takeda 1986, 2012). The accuracy of this technique has already been verified by comparing with standard rheometer measurements with test fluids in which the assumption of a constant shear rate in the narrow gap is confirmed to be satisfied (Yoshida et al. 2019a). In the paper, flow curves of silicon oil and carboxymethyl cellulose (CMC) aqueous solution, which are generally known as Newtonian and shear thinning fluid, were utilized for comparing the results obtained by USR and a conventional torque-type rheometer with plate-plate geometry. As a result, these showed good agreement each other, indicating the accuracy of USR. The best advantage is that USR can elucidate what is happening in the fluid layer, owing to velocity profile measurement. The velocity information represents fluid dynamics and rheology more directly in comparison with the axial torque as an integrated value. This spatially local evaluation expands the scope of rheological evaluation to complex fluids including a variety of polymer solutions (Yoshida et al. 2018, 2019a−c), which are generally ineligible for the conventional torque-type rheometer as these do not meet the flow assumption in the narrow gap. Another notable advantage is an instantaneous spatial evaluation of rheological properties from the velocity profiles at each radial position assuming a different shear rate/strain in the USR vessel. This allows instantaneous evaluations of the rheological properties as, for example, instantaneous flow curves.

The USR measurements thus provide more detailed data of the rheological properties but require a practical representation of the data for reading out and reflecting essential properties of the polymer solutions embedded in the data. To evaluate viscoelasticity with both shear deformation/flow and shear timescale dependence in polymer solutions, we propose a practical representation termed rheology mapping by means of USR. The aim of this study is to establish a method based on USR data for understanding the viscoelasticity in polymer solutions with respect to shear rate, strain, and oscillation frequency. In order to evaluate its efficacy, rheology mapping is here applied to two polymer solutions with different viscoelastic characteristics. One is CMC aqueous solution, which is generally known as a purely viscous and shear thinning fluid. Another is polyacrylamide (PAM) aqueous solution, which is generally considered as a viscoelastic and shear thinning fluid, while it is difficult to evaluate the viscoelasticity of PAM with the standard torque-type rheometer (Jaradat et al. 2012; Goudoulas et al. 2017). These polymer solutions with different molecular weights and concentrations are characterized by the rheology mapping. The obtained results are discussed with previous studies associating the macroscopic properties with microscopic dynamics of polymer coils.

In Sec. 2 following the introduction, theoretical background of the USR for quantitatively evaluating viscoelasticity from the velocity distribution obtained by UVP is briefly explained. The

concept of the rheology mapping is specifically described. Then, general characteristics of the CMC and PAM solutions are detailed and summarized. In Sec. 3, results and discussion on rheological characteristics read from the mapping are denoted. Sec. 4 provides concluding remarks.

2 Methods and test materials

2.1 Ultrasonic spinning rheometry

Schematics of the experimental setup for the USR are shown in Fig. 1. An acrylic cylindrical vessel (radius: $R = 77$ mm) is filled with the test fluid and the top surface is maintained as free. The temperature of the test fluid is kept at 25°C during all the experiments in the thermostatic chamber. An ultrasonic transducer is installed horizontally and $\varepsilon = 15$ mm away from the central axis of the vessel to capture the azimuthal velocity $u_\theta(r, t)$. Oscillation of the vessel is controlled by a stepping motor with the oscillation frequency f_o and maximum rotation angle Θ as the control parameters. The velocity at the side wall of the cylindrical vessel $u_{\mathrm{wall}}(t)$ is defined as $u_{\mathrm{wall}} = U_{\mathrm{wall}}\sin(2\pi f_o t)$, where U_{wall} is the maximum wall velocity $2\pi f_o R\Theta$. The oscillatory shear flow propagating from the cylindrical wall toward the central axis is measured by the UVP, which can acquire the spatiotemporal distribution of the measurement-direction velocity $u_\xi(\xi, t)$ along a line of measurement ξ. Assuming that the flow in the vessel is axisymmetric and that the radial flow is negligible, $u_\theta(r, t)$ is obtained by the geometric relation, $u_\theta = (r/\varepsilon)u_\xi$. The spatial resolution $\Delta\xi$ and temporal resolution Δt are commonly set as $\Delta\xi = O(0.1\ \mathrm{mm})$ and $\Delta t = O(10\ \mathrm{msec})$.

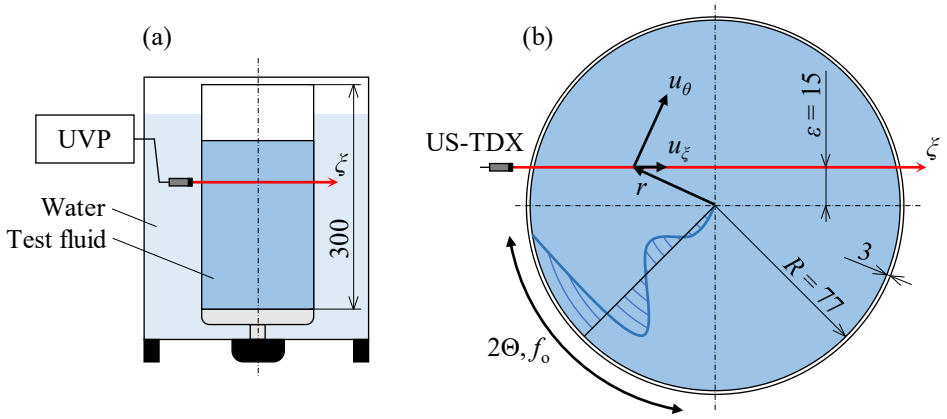

Fig. 1 Schematic diagrams of the experimental setup for capturing spatiotemporal velocity distributions of oscillatory shear flow by the ultrasonic velocity profiler: **a** Side view and **b** top view. Dimensions in [mm].

The rheological properties of a fluid are reflected in the velocity information obtained by the UVP, the properties therefore can be evaluated reversely from the velocity distribution with standard equations of motion. An analytical method was proposed to quantitatively evaluate the viscoelasticity

in a frequency domain to exclude the measurement noise of the UVP (Tasaka et al. 2018). The viscoelasticity is evaluated by this analysis and will appear on the rheology map proposed below, a brief outline is explained here.

The flow field of an axisymmetric one-directional flow in the azimuthal direction must satisfy the Cauchy's equation of motion,

$$\rho \frac{\partial u_\theta}{\partial t} = \frac{\partial \tau}{\partial r} + \frac{2\tau}{r}, \tag{1}$$

where ρ and τ denote the fluid density and shear stress, respectively. To decompose the viscous and elastic contributions to the shear stress, the Maxwell model is utilized locally to describe the relation between τ and u_θ as,

$$\tau + \frac{\mu}{E}\frac{\partial \tau}{\partial t} = \mu\left(\frac{\partial u_\theta}{\partial r} - \frac{u_\theta}{r}\right), \tag{2}$$

where μ and E denote the viscosity coefficient and elastic modulus, respectively. Here, adopting Maxwell model locally assumes linear viscoelasticity for a given local effective shear rate, but it can evaluate nonlinear behavior against variations of the effective shear rate distributing in the radial direction. In other words, the viscosity coefficient and elastic modulus of the model are determined depending on the radial position as the shear rate amplitude takes maximum value on the cylindrical wall and decreases toward the central axis. In addition to this, odd harmonics in the velocity intensity spectrum calculated from the velocity data obtained at each radial position have not been detected even under large amplitude oscillatory shear (LAOS) in the experiments denoted below, so it is unnecessary to consider the nonlinear viscoelasticity in one oscillation cycle at each radial position. The theory of USR itself can be extended for evaluating nonlinear viscoelasticity from the odd harmonic components in future.

A Fourier transform (symbol of operation: ^) is performed on Eqs. (1) and (2) to remove the measurement noise of the UVP and extract only the dominant frequency component corresponding to the oscillation frequency $f_o = \omega_o/2\pi$. The following cost function $F(\mu, E; r)$ is defined as a square residual of both sides of Eq. (1) which is used to apply the Fourier transform,

$$F\left(\mu, E; r\right) = \left| i\omega\rho\hat{u}_\theta - \left(\frac{\partial}{\partial r} + \frac{2}{r}\right)\hat{\tau}\right|^2_{\omega=\omega_o}. \tag{3}$$

The combination of μ and E minimizing the cost function is the optimal for expressing viscoelasticity at the radial position. Solving the optimization problem at each radial position r, $\mu(r)$ and $E(r)$ are obtained. The phase lag of the viscoelasticity δ is defined as $\tan\delta = E/\mu\omega_o$. This is an indicator to quantify the viscoelasticity where $\delta = \pi/2$ rad stands for a purely viscous material, $\delta = 0$ rad for a purely elastic one and δ taking values between the two for a viscoelastic material. As E takes values from zero to infinity, it is difficult to solve the optimization problem, and μ and δ are utilized instead

of μ and E.

The spatiotemporal distribution of the simple shear rate $\dot{\gamma}(r, t)$ is calculated from $u_\theta(r, t)$ as

$$\dot{\gamma}(r,t) = \left(\frac{\partial}{\partial r} - \frac{1}{r} \right) u_\theta(r,t) . \tag{4}$$

The effective shear rate $\dot{\gamma}_{\mathrm{eff}}(r)$ and shear strain $\gamma_{\mathrm{eff}}(r)$ are respectively defined as effective values of $\dot{\gamma}(r, t)$ and $\gamma(r, t)$ at each radial position, being respectively defined as the representative shear rate and strain. It should be noted that μ and E take different values for each r in a non-Newtonian fluid, as $\dot{\gamma}_{\mathrm{eff}}$ takes different values depending on radial position.

As USR is based on the velocity information obtained by UVP, the applicable and measurable ranges of USR are deeply related to these of UVP, whose measurable maximum velocity and time resolution are several hundred mm/s and around 10 ms, respectively. The available range of the shear rate is therefore up to around 50 s^{-1}. Requirement on discretization of a period of cylinder oscillation by at least ten points with the time resolution above gives the limitation on the oscillation frequency up to around 10 Hz. As for the available range of the viscosity, the minimum kinematic viscosity is limited to $O(1\ \mathrm{mm}^2/\mathrm{s})$ as the thickness of the viscous layer on the wall evaluated by $(\nu/2\pi f_\mathrm{o})^{1/2}$ is smaller than the spatial resolution of UVP, $O(1\ \mathrm{mm})$, where ν represents a kinematic viscosity of the test fluid. USR utilizes space-time velocity information and requires time delay of the velocity fluctuation in the radial direction in the cylindrical vessel. The thickness of the viscous layer therefore should be smaller than the radius of the vessel R, restricting the maximum viscosity to be smaller than several thousand mm^2/s.

2.2 Basic concept for the rheology mapping based on USR

The USR makes it possible to evaluate the viscoelasticity with shear rate dependence even with fixed oscillation parameters (f_o, Θ), because of the radial distributions of the shear rate amplitudes in the cylindrical vessel. The frequency dependence of the viscoelasticity can then be evaluated effectively by stepwise increases in the oscillation frequency f_o. In all the experiments for the investigation in this paper, f_o is increased from 0.2 Hz to 3.0 Hz in increments of 0.2 Hz. The maximum angle of rotation Θ corresponding to a f_o is set so that the maximum wall velocity U_{wall} is a constant under all the f_o conditions. The following rheology mapping inspired by the classical Pipkin diagram (Pipkin 1986) is proposed as a method to disassemble the complex data in the information of the viscoelasticity obtained by the above series of experimental operations. The viscosity coefficient μ and phase difference δ are summarized by contours on a two-dimensional map in which the axes correspond to f_o and the effective shear rate $\dot{\gamma}_{\mathrm{eff}}$, respectively (Fig. 2a). The relation $\dot{\gamma}_{\mathrm{eff}} = 2\pi f_\mathrm{o} \gamma_{\mathrm{eff}}$ holds along $\dot{\gamma}_{\mathrm{eff}}$, f_o and the effective shear strain γ_{eff}. The group of contour curves of γ_{eff} matches a group of straight lines passing through the origin of the map (Fig. 2a). A contour approaches the vertical axis as γ_{eff} increases. The map therefore is a comprehensive reflection of the dependence of the viscoelasticity on $\dot{\gamma}_{\mathrm{eff}}$, γ_{eff},

and f_o. In the map, the vertical axis given by the present rheology mapping is $\dot{\gamma}_{eff}$, while the Pipkin diagram (Pipkin 1986) adapts strain amplitude and frequency for the axes.

For ease of understanding the rheology mapping, three ideal examples showing simplified rheological properties as Newtonian, shear thinning without and with elasticity are considered and presented in Figs. 2b–2d. The first example showing a Newtonian viscosity will be represented as a monochrome in both the map representations of δ and μ (Fig. 2b). The second example showing shear thinning without elasticity is represented as colored map patterns in Fig. 2c. The monochrome in the map of δ means that the fluid is purely viscous regardless of the values of $\dot{\gamma}_{eff}$, γ_{eff}, and f_o, while the color variations in the map representing μ expresses shear thinning characteristic. The third example showing shear thinning with elasticity is represented as the colored map patterns in Fig. 2d. In this ideal case, viscoelasticity varies from elastic to viscous essentially as γ_{eff} increases. The color variations in the map representation of μ expresses the γ_{eff}-dependent shear thinning characteristic. In this way, the dependence of viscosity and degree of viscoelasticity can be directly and comprehensively identified.

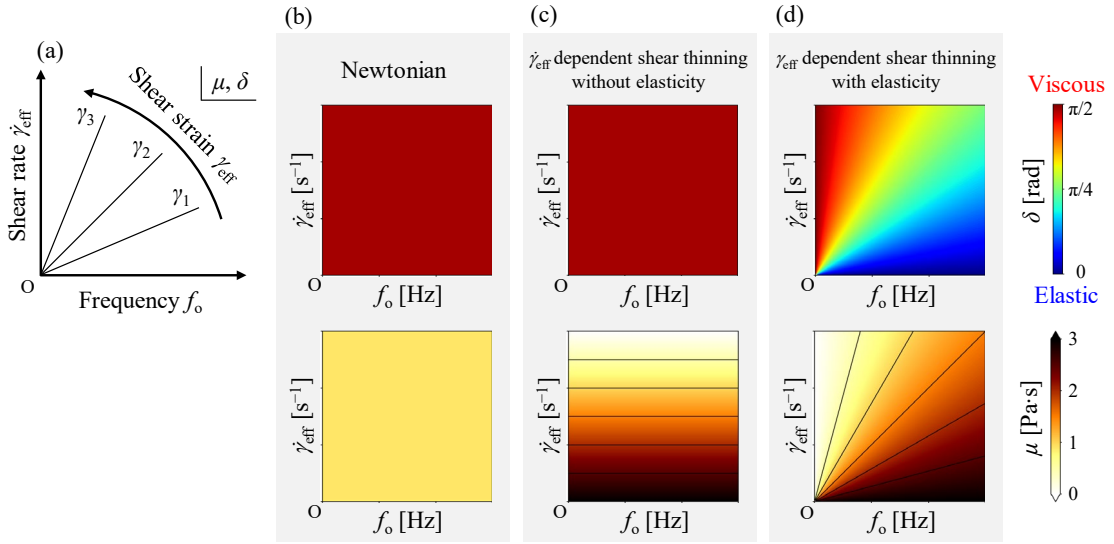

Fig. 2 The concept of the rheology mapping for evaluating the dependence of viscoelasticity on shear rate $\dot{\gamma}_{eff}$, strain γ_{eff}, and frequency f_o: **a** definition of each axis, and three ideal examples showing simplified rheological properties as **b** Newtonian, **c** shear thinning without elasticity, and **d** γ_{eff} dependent shear thinning with elasticity.

2.3 Characteristics of the test fluids

Two kinds of polymer solutions are examined by the present rheology mapping. The first is a carboxymethyl cellulose (CMC) aqueous solution (Daicel Miraizu Co. Ltd., Japan, Molecular weight: 2.0×10^6 g/mol), which is widely used as a thickener in cosmetics and pharmaceuticals. The rheological properties of the solution have been evaluated by standard torque-type rheometers in many

reports (Kulicke et al. 1996; Benchabane and Bekkour 2008), and the efficacy of the measurements have also been examined by visualizing the flow in the narrow gap of a rheometer (Yoshida et al. 2019a). The CMC solution is generally known as purely viscous and shear thinning fluid. In the present study, CMC aqueous solutions in three different concentrations (0.5, 1.0 and 1.5 wt.%) are examined to investigate how variations of the concentration are represented by the rheology mapping. The properties identified in previous studies will be detailed with the map, and additional characteristics discovered in the comprehensive evaluation will be discussed. In the experiments, small amounts of fine spherical particles (CHP20P, Mitsubishi Chemical Co. Ltd., Japan), of density and mean diameter 1.01 g/mL and 75−150 μm, are mixed little into all the test fluids as tracer particles for the UVP measurements. The added particles have weak chemical reactivity so as not to affect the rheological properties. Furthermore, density difference between the particles and the aqueous solutions is sufficiently small to be regarded as neutral buoyancy. Stokes number is estimated to be several orders of magnitude lower than unity, indicating sufficient performance as tracer particles.

The second test fluid is polyacrylamide (PAM) aqueous solution (MT AquaPolymer Co. Ltd., Japan, Molecular weight: 1.3×10^7 g/mol). The molecular weight is 6.5 times that of the CMC. The PAM solution is generally regarded as viscoelastic and shear thinning fluid (Ghannam and Esmail 1998; Lewandowska 2007). In the PAM solution, shear banding occurs even inside the narrow gap of standard rheometers. Careful attention therefore must be paid to the specifics of the measurements as demonstrated later in this section, to ensure that inaccuracies in the evaluated viscoelasticity are accounted for. As with the CMC solutions, PAM aqueous solutions with three different concentrations (0.5, 1.0 and 1.5 wt.%) are examined here.

To validate and demonstrate sufficient applicability of viscoelasticity evaluation by USR to complex fluids, viscosity evaluation of 1.0 wt.% PAM solution by a standard torque type rheometer (MCR 102, Anton Paar) with cone and plate geometry was conducted for comparison with USR. The results are summarized in Fig. 3, where the strain amplitude sweep mode is utilized under the oscillation frequency $f_o = 1.0$ Hz as a representative. Storage modulus G' and loss modulus G'' measured by the rheometer are converted to viscosity coefficient μ and phase difference of viscoelasticity δ for comparison with USR. In addition, the series of strain amplitudes in the large amplitude oscillatory shear (LAOS) test is also converted to the effective shear rate $\dot{\gamma}_{\mathrm{eff}}$. The results of the LAOS test are displayed up to $\dot{\gamma}_{\mathrm{eff}} = 10\ \mathrm{s}^{-1}$, because accurate measurement could not be performed for further high strain amplitudes due to an abnormal vibration phenomenon probably caused from the shear banding or wall slip. On the other hand, USR is practical to such complex fluids as it determines actual profiles of local shear rates in the evaluation of viscoelasticity. The result of USR is also shown in Fig. 3. Comparing the results, it can be confirmed that they have the same tendency and good

coincides in the overlap region of $\dot{\gamma}_{\mathrm{eff}}$. Based on the viscosity and delta curves obtained by USR, the reason for the abnormal vibration at $\dot{\gamma}_{\mathrm{eff}} = 10^1\ \mathrm{s}^{-1}$ in the LAOS test might be that the shear banding was formed in the narrow gap due to the rapid change in the viscoelasticity at this shear rate as shown by the curves evaluated by USR in Fig. 3. It should be noted that the agreement between the two results in the overlap range reinforces the validity of the viscoelasticity evaluation by USR.

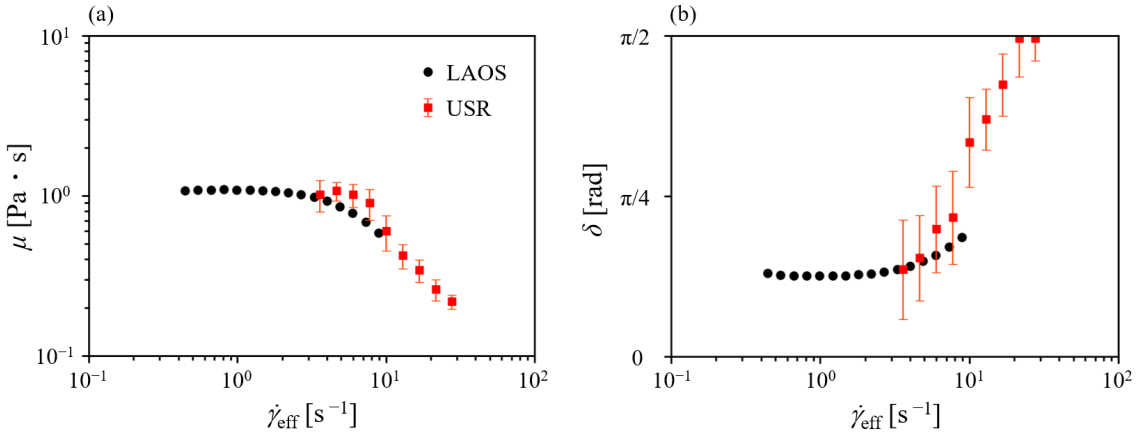

Fig. 3 Comparison of viscoelasticity evaluated by USR and LAOS test of the torque-type rheometer for the PAM 1.0 wt.% solution: Shear rate dependence of (a) viscosity coefficient μ, and (b) phase difference of viscoelasticity δ, where the oscillation frequency is $f_{\mathrm{o}} = 1.0$ Hz.

3 Results and discussion

The following section is a comprehensive evaluation of the dependence of the viscoelasticity of the CMC and PAM solutions on the shear rate, strain, and frequency based on the ideas of the rheology mapping. Notable characteristics of the two solutions are detailed independently for each of the solutions in Secs. 3.1 and 3.2, respectively. The obtained results are further discussed based on the microscopic dynamics of polymer coils in Sec. 3.3.

3.1 Viscous dominant fluid: the carboxymethyl cellulose aqueous (CMC) solutions

The CMC solutions with different concentrations (0.5, 1.0, 1.5 wt.%) were prepared in the cylindrical vessel as detailed in Sec. 2.1. For the different frequencies f_{o} applied to the vessel, the flow velocity distributions were measured by the UVP, and the rheological properties were evaluated with the procedures of the USR. At the oscillation parameters ($f_{\mathrm{o}} = 1.0$ Hz and $\Theta = \pi/2$ rad, $U_{\mathrm{wall}} = 760$ mm/s), Fig. 4 indicates the time variations of instantaneous radial profile of u_θ. The axes show the cycle periods of the oscillation and the normalized radial coordinates, while the contours represent the

measured velocity in the azimuthal direction. These spatiotemporal distributions show that the oscillatory shear flow driven by the cylindrical wall (r/R = 1.0) propagates toward the central axis with a time delay (diagonal patterns on the distribution) and attenuation (lowering in the velocity amplitude away from the wall). For the 0.5 wt.% CMC solution the flow is established at $r/R > 0.75$, as the thickness of a viscous layer at the cylinder wall. The degree of the time delay and attenuation decreases as the CMC concentration increases: the viscosity increases as the concentration increases. As USR evaluates the rheological properties based on these velocity distributions, only the radial range with high accuracy is used for the analysis. UVP Monitor model-Duo (Met-Flow, S.A., Switzerland) used in the experiments utilizes 8-bit digital signal processor, therefore, the velocity resolution Δu_ξ is defined as $\Delta u_\xi = U_{max}/256$, where U_{max} is the maximum measurable velocity set by UVP. For this reason, the radial range with velocity intensity comparable to the velocity resolution is not used in the analysis as shown by the dotted line in Fig. 4a. Spatial resolution of UVP is determined by the size of the ultrasonic pulse wave having cylindrical shape. The spatial resolution $\Delta\xi$ along the axis ξ is constant, but as the radial position becomes smaller, particularly smaller than r/R = 0.5, the ultrasonic pulse wave straddles in the radial direction, deteriorating the spatial resolution Δr. The radial range of $r/R < 0.5$ is therefore excluded in the analysis as shown in Figs. 4b and 4c.

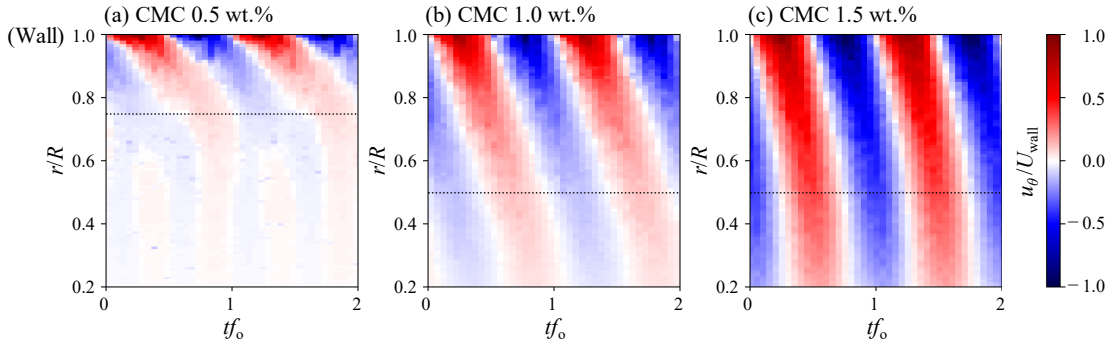

Fig. 4 Spatiotemporal velocity distributions obtained by the UVP for the CMC solutions with different concentrations: **a** 0.5 wt.%, **b** 1.0 wt.%, and **c** 1.5 wt.%, for the set oscillation parameters of f_o = 1.0 Hz and $\Theta = \pi/2$ rad.

The rheological properties of the CMC solutions were examined for different concentrations (0.5, 1.0, and 1.5 wt.%) following the procedures of the USR as explained in Sec. 2.1. The results of the rheology mapping for the CMC solutions are summarized in Fig. 5. The upper and lower panels respectively indicate the phase lag δ and the viscosity coefficient μ, represented by the contour. Since the thickness of viscous layer is too thin to evaluate the properties considering the spatial resolution of the UVP, the rheological evaluations are limited to within 1.0 and 2.0 Hz in the 0.5 and 1.0 wt.% solutions, respectively.

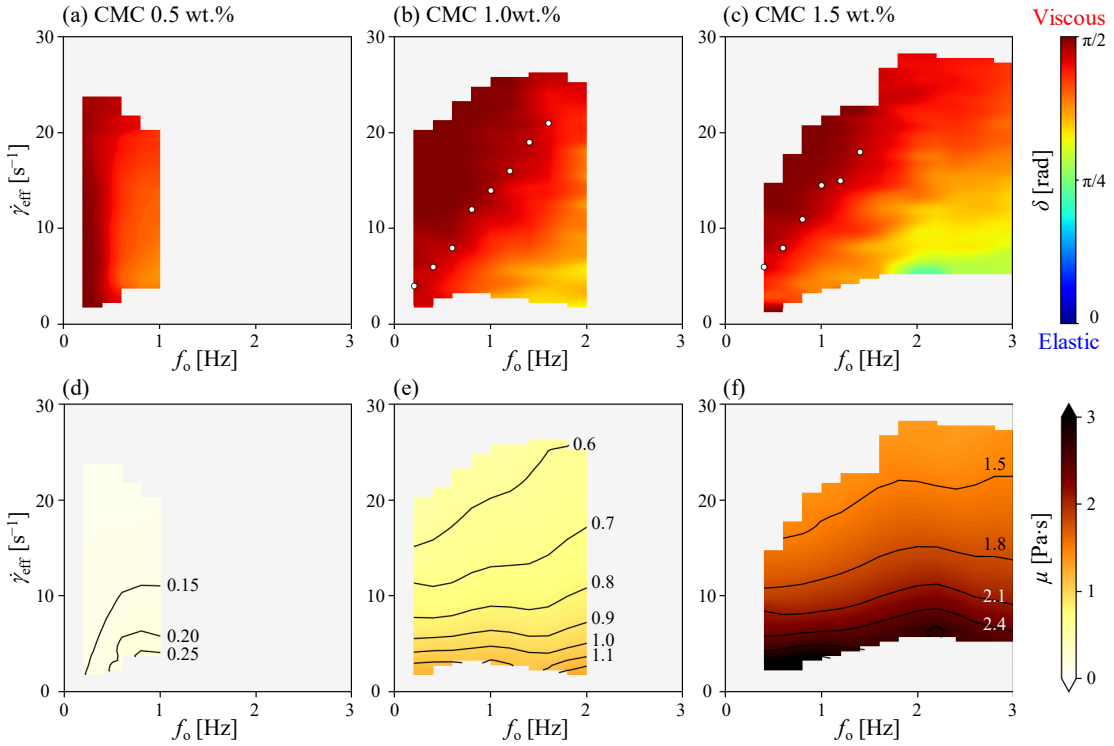

Fig. 5 Rheology mapping for the CMC solutions with different concentrations: **a**–**c** and **d**–**f** indicate the distribution of phase differences δ and viscosity coefficients μ, respectively. White dots in **b** and **c** represent the critical shear rate $\dot{\gamma}_{\mathrm{eff,\,c}}$ at each oscillation frequency f_o.

The phase lag δ in the 0.5 wt.% case (Fig. 5a) shows a purely viscous behavior at the $f_\mathrm{o} \leq 0.5$ Hz range and changes to viscoelastic fluid at the opposite range. In Fig. 5d, μ assumes a constant value at the lowest frequency $f_\mathrm{o} = 0.2$ Hz, representing a Newtonian-like fluid behavior, and shear thinning characteristic emerges weakly as f_o increases.

At the higher concentrations, 1.0 and 1.5 wt.%, δ widely varies depending on f_o and $\dot{\gamma}_\mathrm{eff}$. The CMC solutions are generally seen as purely viscous fluids, but the results also express the elasticity as depending on $\dot{\gamma}_\mathrm{eff}$ and f_o. White dots superimposed on the panels in Figs. 5b and 5c represent the critical shear rates $\dot{\gamma}_{\mathrm{eff,\,c}}$, showing $\delta \approx \pi/2$ rad at each f_o. The critical shear rates are replotted in Fig. 6 with the standard deviations. These plots form a straight line passing through the origin of the map, corresponding to a contour line for the effective shear strain γ_eff. The critical shear strains determined by the least squares method are $\gamma_{\mathrm{eff,\,c}} = 210\%$ and 206% at the 1.0 and 1.5 wt.% concentrations, respectively without any significant difference between the two values. The solutions completely lose elasticity when γ_eff exceeds $\gamma_{\mathrm{eff,\,c}}$.

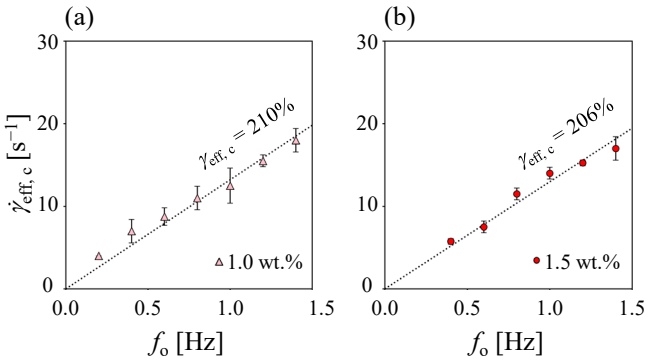

Fig. 6 Deviation of the critical shear rate $\dot{\gamma}_{\mathrm{eff,c}}$ at various oscillation frequencies f_o for the CMC solutions with different concentrations: **a** 1.0 wt.% and **b** 1.5 wt.%; the error bars indicate standard deviations and the dotted lines are the regression curves $\dot{\gamma}_{\mathrm{eff,c}} = 2\pi f_o \gamma_{\mathrm{eff,c}}$ for determining the critical shear strain $\gamma_{\mathrm{eff,c}}$.

Focusing on the distributions of μ for the 1.0 and 1.5 wt.% solutions as shown in Figs. 5e and 5f, the shear thinning characteristic is confirmed at any f_o. It is notable that the contour lines of μ are generally horizontal meaning that the viscosity strongly depends on $\dot{\gamma}_{\mathrm{eff}}$, and not on γ_{eff} and f_o. In the previous paper (Yoshida et al. 2019a), the agreement between the viscosity curve evaluated by USR in the oscillatory shear and the one evaluated by the torque-type rheometer in the steady shear was confirmed, which reinforces the validity of this characteristic of the CMC solutions. These remarkable characteristics will be discussed further in Sec. 3.3.

3.2 Viscoelastic fluid: the polyacrylamide (PAM) aqueous solutions

The PAM solutions with different concentrations (0.5, 1.0, 1.5 wt.%) are examined based on the same procedures as detailed in Sec. 3.1. The spatiotemporal velocity distributions were measured as shown in Fig. 7, where the oscillation parameters are representatively given as $f_o = 1.0$ Hz and $\Theta = \pi/2$ rad. Compared with the distributions in the CMC solutions in Fig. 4, those of the PAM solutions are clearly different. The oscillatory shear flow propagates without any phase lag near the central axis as shown in Figs. 7b and 7c, showing that the solutions are subject to a yield stress. As explained in Sec. 3.1, the radial range in which the velocity intensity is comparable to the velocity resolution of UVP is not utilized as shown in Fig. 7a and 7b for assuring accuracy of the velocity information. Furthermore, as USR evaluates viscoelasticity under the oscillatory shear flow, the region of rigid body rotation without considerable radial phase delay is unexamined. The region unexamined depends on the concentration and shown by the dotted line in Fig. 7c.

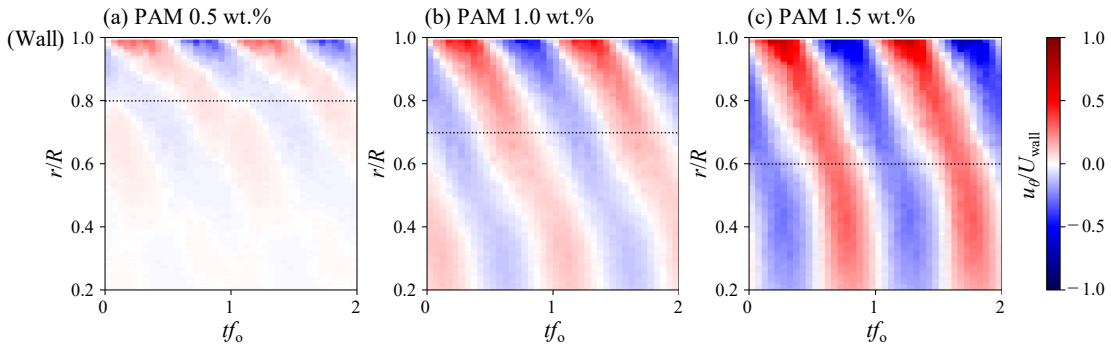

Fig. 7 Spatiotemporal velocity distributions obtained by the UVP in the PAM solutions with different concentration: **a** 0.5 wt.%, **b** 1.0 wt.%, and **c** 1.5 wt.%, for the set parameters, f_o = 1.0 Hz and $\Theta = \pi/2$ rad.

The results of the rheology mapping with the PAM solutions are shown in Fig. 8. In the 0.5 wt.% solution, viscoelasticity clearly appears at the $f_o \geq 0.8$ Hz range in Fig. 8a, while the CMC solution with the same concentration is viscous with weak elasticity as shown in Fig. 5a. Focusing on the distribution of μ in Fig. 8(d), the shear thinning characteristics appear at all f_o values, and there are no Newtonian regions like those observed in the CMC solution with the same concentration.

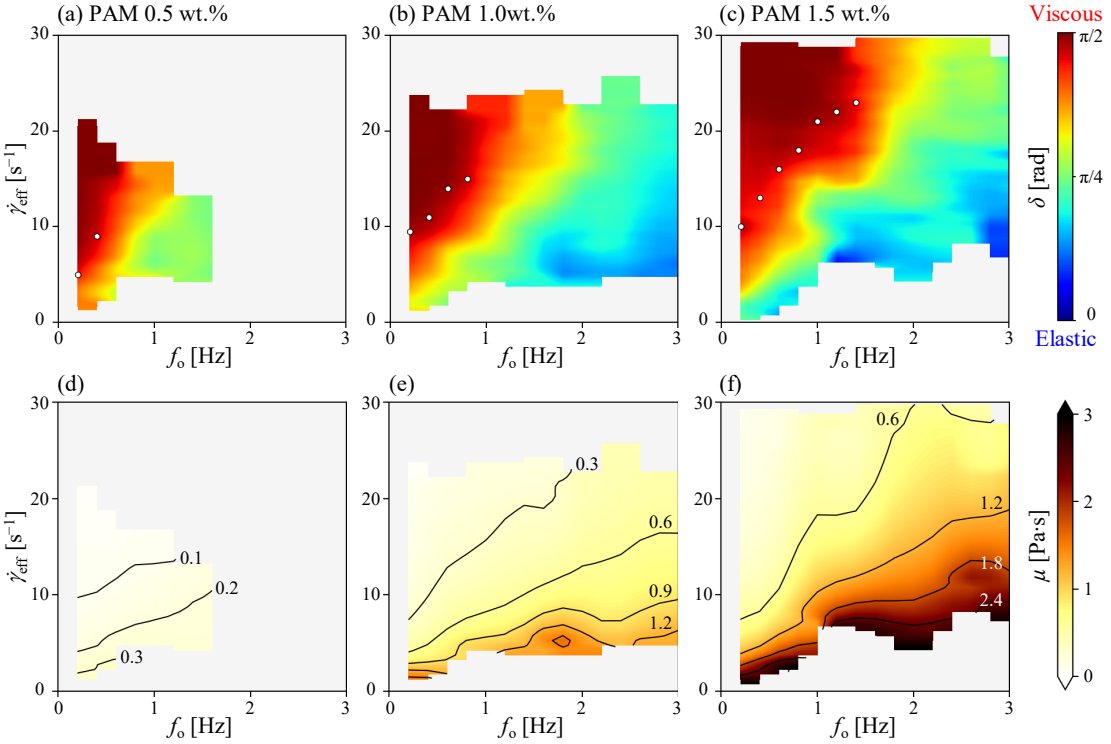

Fig. 8 Rheology mapping for the PAM solutions with different concentrations: **a**–**c** and **d**–**f** indicate distributions of the phase difference δ and viscosity coefficient μ, respectively. White dots in **a**–**c** represent the critical shear rate $\dot{\gamma}_{\mathrm{eff,\,c}}$ at each oscillation frequency f_o.

In the 1.0 and 1.5 wt.% solutions in Figs. 8b and 8c, the measurable range in f_o is widened because of the increased apparent viscosity of the solutions. In these two solutions, the dominant region of elasticity is wider than that of the 0.5 wt.% solution at the $f_o \geq 1.0$ Hz range. It must be noted that δ approaches $\pi/2$ rad (i.e. purely viscous) as the effective shear strain γ_{eff} increases. Although the PAM solution is generally known as a viscoelastic fluid, it changes to purely viscous with increasing γ_{eff}. As also mentioned in Sec. 3.1, the viscoelasticity shifts from viscous to elastic in a wide range of the map. The critical shear rates $\dot{\gamma}_{eff,c}$ in Figs. 8a–8c are replotted in Fig. 9 with the standard deviations. The graph shows that $\dot{\gamma}_{eff,c}$ increases as the concentration increases. Compared with the $\gamma_{eff,c}$ of the CMC solutions as shown in Fig. 6, that of the PAM solutions assumes larger values with around 400% (Fig. 9).

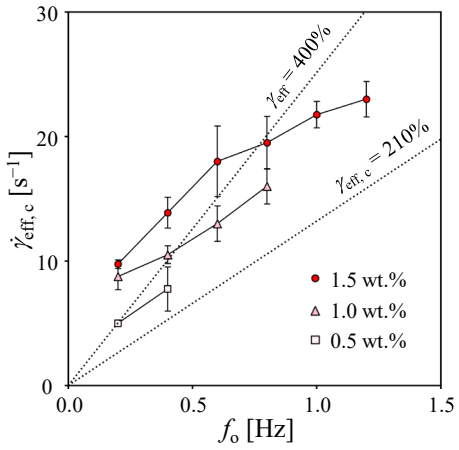

Fig. 9 Deviation of the critical shear rate $\dot{\gamma}_{eff,c}$ at each oscillation frequency f_o for the PAM solutions with different concentrations, error bars indicate standard deviations. The lower dotted line represents the critical shear strain $\gamma_{eff,c}$ = 210% evaluated in the CMC solutions (Fig. 6).

Focusing on the distributions of μ for the 1.0 and 1.5 wt.% solutions (Figs. 8e and 8f), the pattern of the contour lines is very different from that of the CMC solutions (Figs. 5e and 5f). While that of the CMC solutions is horizontal, that of the PAM solutions can be regarded as forming a group of lines which almost all pass through the origin, corresponding to a group of contour lines for γ_{eff}. The viscosity of the PAM solutions therefore strongly depends on γ_{eff}.

3.3 Evaluation of the rheology mapping

3.3.1 CMC aqueous solutions

The rheological properties displayed by the rheology mapping are discussed here in association with the microscopic dynamics of polymer coils. For the 0.5 wt.% CMC solution in Fig. 5d, the $\dot{\gamma}_{eff}$

dependence of μ clearly shifts from Newtonian towards shear thinning at around f_o = 0.5 Hz. The major causes of the shear thinning characteristics in polymer solutions are generally explained by shear induced structures such as disentanglement, stretch, or increases in the orientation of the polymer coils in the direction of the flow (Schramm 2000; Deshpande et al. 2010; Rao 2014). The 0.5 wt.% concentration CMC solution is estimated to be in a semi-dilute non-entangled regime (Benchabane and Bekkour 2008), that is, the dispersed polymer coils in the water are individually dispersed without contact each other. Under oscillatory shear flows, the difference between the timescale of the oscillatory shear flow t_f (i.e. reciprocal of the oscillation frequency f_o) and the major relaxation time t_r of the polymer coil would determine the characteristic shift from a Newtonian to a non-Newtonian regime. When t_f is shorter than t_r, the dispersed polymer coils always keep stretched, due to insufficient relaxation during a single oscillation cycle. The degree of the stretch affects the flow resistance viewed microscopically according to Dunstan *et al*. (2004). The shear thinning characteristics observed at the range of $f_o \geq 0.5$ Hz in Fig. 5d may then be considered as a result of the stretching of the dispersed polymer coils, whose degree of the stretching depends on $\dot{\gamma}_{eff}$. Under the opposite condition ($t_f > t_r$), the viscosity coefficient is not dependent on $\dot{\gamma}_{eff}$ due to insufficient stretching of the polymer coil, that is, the shear induced structure is not maintained throughout the oscillation cycle. As the result, the 0.5 wt.% concentration CMC solution has Newtonian regime in the region of $f_o \leq 0.5$ Hz in Fig. 5d. These considerations are also supplemented by the results shown in Fig. 5a, indicating the clear boundary between purely viscous and viscoelastic at f_o = 0.5 Hz.

With higher concentrations of the CMC solutions (1.0 and 1.5 wt.%), shear thinning characteristic emerges at all the f_o conditions. As the concentration increases, polymer coils become overlapped (Graessley 1980), and form enhanced segments of polymer coils, accompanying increased relaxation times of the segments. The boundary between the Newtonian and shear thinning regimes suggested at 0.5 Hz in Fig. 5d, therefore, shifts to the lower frequency side, and no Newtonian regime is observed in Figs. 5e and 5f. In addition to the shear thinning characteristic observed at all the f_o conditions, it is notable that the viscosity of the CMC solutions with 1.0 and 1.5 wt.% concentrations strongly depends on $\dot{\gamma}_{eff}$ as mentioned in Sec. 3.1. It was experimentally confirmed that orientation and distortion of a polymer coil vary depending on the applied shear rate and that this causes the shear thinning characteristic in steady shear flows (Dunstan et al. 2004). This also holds for the oscillatory shear flow and the viscosity of the CMC solutions depend most strongly on $\dot{\gamma}_{eff}$, and less or not on γ_{eff} and f_o as shown in Figs. 5e and 5f. In addition, it is notable that the 1.0 and 1.5 wt.% concentration CMC solutions have almost the same critical shear strain as shown in Fig. 6. This means that the polymer coil yields or entanglement of them is resolved, and elasticity does not develop with γ_{eff} approaching to $\gamma_{eff,\,c}$. As the concentration increases, the number of entanglements between polymer coils increases and greater stress is required to disentangle the structures (Kulicke et al. 1996). It must be noted, however, that the shear strain required for the disentanglement does not depend on the concentration

as shown by the results in Fig. 6. This is a new finding, and one that can be read from the novel representations by the rheology mapping in Figs. 5b and 5c.

3.3.2 PAM aqueous solutions

For the 0.5 wt.% concentration PAM solution, shear thinning characteristic is confirmed at all the f_o conditions as shown in Fig. 8d, while the CMC solution with the same concentration shows the clear shift from Newtonian to shear thinning characteristic at f_o = 0.5 Hz as shown in Fig. 5d. Molecular weight of the PAM is 6.5 times that of the CMC, polymer coils in the 0.5 wt.% PAM solution therefore have longer relaxation times than those of the 0.5 wt.% CMC solution. The boundary between the Newtonian and shear thinning regimes shifts to the lower frequency side than f_o = 0.5 Hz and no Newtonian regime is observed. As for the δ distribution shown in Fig. 8a, δ takes lower values than that of the CMC solutions in Fig. 5a−5c at each f_o and $\dot{\gamma}_{eff}$. Viscoelasticity is more pronounced in the PAM solution. When the molecular weight increases, the elastic effect of the entanglement and the polymer coil itself is stronger than the thickening effect of the number of polymer coils.

With thicker PAM solutions (1.0 and 1.5 wt.%), it is notable that μ decreases as γ_{eff} increases. This trend is also observed in the δ distributions as shown in Figs. 8b and 8c. The strong dependence of μ and δ on γ_{eff} can be understood as an effect of the disentanglement of the polymer coils from the applied γ_{eff}. Strongly entangled polymer coils cause elasticity and high viscosity. Entanglements of polymer coils are gradually disentangled according to the applied γ_{eff}, and elasticity and viscosity decrease, closely depending on γ_{eff}. The main factor in the shear thinning of the CMC solutions is considered to be the orientation of single polymer coils as mentioned. However, for these two PAM solutions, the remaining entanglements do not allow single polymer coils to orient alone, and the disentanglement of the polymer coils may be surmised to be the dominant factor in the shear thinning characteristics here. Based on the experiments conducted by Kulicke and Porter (1980) comparing steady and dynamic shear viscosities of PAM solutions, they considered that shear strain, not frequency, is responsible for disentangling the polymer coils. The increasing δ and decreasing μ as γ_{eff} increases would therefore quantitatively support their deduction. In addition, $\dot{\gamma}_{eff,\,c}$ increases with the concentration as shown in Fig. 9. It is considered that not only the overlap between the polymers increases as the concentration increases, but also a stronger entanglement is formed. As the result, yield and disentanglement of the polymer coils are less likely to occur, and $\dot{\gamma}_{eff,\,c}$ is increased with the concentration.

3.4 Advantages of the rheology mapping

As shown in the demonstrations of the two types of the polymer solutions above, the current rheology mapping can relatively easily and quantitatively show how the generally known micro dynamics are reflected in the macro rheology. The rheological properties suggested in other literatures (e.g., Kulicke

and Porter 1980; Dunstan et al. 2004; Yoshida et al. 2019a) have been quantitatively clarified. For example, it was clarified that the CMC solution generally known as a purely viscous fluid has viscoelasticity below the critical shear strain. If the frequency sweep test is performed with a strain amplitude larger than the critical one, this characteristic will be overlooked. Furthermore, displaying the shear rate as the vertical axis, not the shear strain as like the Pipkin space, makes it possible to elucidate which of the shear rate, strain, and frequency is the essential factor to change the viscoelasticity, as was clarified in the demonstrations of the CMC and PAM solutions. Similar maps also can be created based on the LAOS test of the torque-type rheometer, and strain-softening/stiffening, purely viscous shear thinning/thickening etc. have been successfully characterized (Ewoldt et al., 2008). However, the method has limitations, for example, the extraordinarily severe symmetry assumptions often lead to confusion when it comes to data interpretations (Pan and Germann, 2020). Furthermore, it should be noted deeply in mind that the fluid to which the method can be applied is exactly limited to that of the torque-type rheometer. Particularly in polymer solutions with high molecular weight such as the PAM solutions mentioned in Sec. 3.3.2, the solution easily causes shear-banding inside the narrow gap of the rheometer, giving bias errors to the torque measurement value that should originally reflect the viscoelasticity. The current rheology mapping based on the spatially local evaluation allows the PAM solution to be compared on the same basis as the CMC solution.

Fluids to be evaluated for rheological characteristics would be further complicated in food, chemical, and energy industries. As the viscoelasticity of these complex fluids changes variously depending on the shear rate, strain, and frequency, such map representation is indispensable for characterizing the fluids. Owing to the local evaluation based on the velocity information obtained by UVP, USR has great advantages on evaluation of not only the polymer solutions but also complex and multiphase fluids. The rheology mapping based on USR will be a practical tool for studies of fluid mechanics aiming to examine flows of complex fluids. There is no intention of deciding which is better, the conventional torque-type rheometer or USR. By utilizing these in a complementary manner, it will be achieved to expand the scope of rheological evaluation to meet diversifying demand from the various industry fields.

4 Conclusions

We proposed a practical map representation based on ultrasonic spinning rheometry, termed rheology mapping, for comprehensively evaluating the dependence of viscoelasticity on the effective shear rate $\dot{\gamma}_{\mathrm{eff}}$, strain γ_{eff} and oscillation frequency f_{o} of the shear acting on tested fluids. Based on USR, the excellent applicability of the method to complex fluids including a wide variety of polymer solutions was ensured. In order to verify the practicality of the present rheology mapping, it was applied to two

kinds of polymer solutions with different rheological characteristics: carboxymethyl cellulose (CMC) and polyacrylamide (PAM) aqueous solutions. The property of the former has been known as a purely viscous and shear shinning fluid, and the latter as a viscoelastic and shear thinning fluid while it has also been recognized that it presents difficulties for measurements in the standard rheometer due to shear banding, elastic instability, and other factors.

The rheology mapping characterized the properties of the CMC and PAM solutions as they change among viscous, viscoelastic, and elastic, widely depending on the applied $\dot{\gamma}_{\mathrm{eff}}$, γ_{eff}, and f_{o}. It was clearly shown that the CMC solution, which is generally considered as a purely viscous fluid, exhibits viscoelasticity below a critical shear strain. It was also confirmed that both the CMC and PAM solutions have shear thinning effects, as it is often observed in polymer solutions. Notable characteristics that may be read from the rheology mappings are the clear dependence of the viscosity of the solutions: the CMC solutions on the $\dot{\gamma}_{\mathrm{eff}}$ and the PAM solutions on the γ_{eff}. Possible explanations for this are considered based on the dynamics of polymer coils as predicted in other polymer investigations. Dominant factors of the shear thinning of the CMC and PAM solutions are, respectively, the orientation and disentanglement of the constituent polymer coils. The present rheology mapping suggests that it is essential to define viscosity as a function of $\dot{\gamma}_{\mathrm{eff}}$ for the CMC solutions and as a function of γ_{eff} for the PAM solution as a rheology model in a numerical simulation of oscillatory shear flows for these compounds. These will be related with microstructures by utilizing Rheo-SANS or Rheo-Optics, for example, orientation of dispersed polymer coils (Wagner 1998; van der Linden et al. 2003; Eberle and Porcar 2012).

Acknowledgements

This work was supported by JSPS KAKENHI Grant Numbers JP19H02057 and 18KK0105, and by f^3 Engineering Education and Research Center, Faculty of Engineering, Hokkaido University.

References

Benchabane A, Bekkour K (2008) Rheological properties of carboxymethyl cellulose (CMC) solutions. Colloid Polym Sci 286:1173−1180

Clasen C, Kulicke WM (2001) Determination of viscoelastic and rheo-optical material functions of water-soluble cellulose derivatives. Prog Polym Sci 26:1839−1919

de Souza Mendes PR, Alicke AA, Thompson RL (2014) Parallel-plate geometry correction for transient rheometric experiments. Appl Rheol 24:1−10

Krishnan JM, Deshpande AP, Kumar S (eds) (2010) Rheology of complex fluids. Springer-Verlag New York

Divoux T, Fardin MA, Manneville S, Lerouge S (2016) Shear banding of complex fluids. Annu Rev Fluid Mech 48:81−103

Dunstan DE, Hill EK, Wei Y (2004) Direct measurement of polymer segment orientation and distortion in shear: semi-dilute solution behavior. Polymer 45:1261−1266

Eberle AP, Porcar L (2012) Flow-SANS and Rheo-SANS applied to soft matter. Curr Opin Colloid Interface Sci 17:33−43

Ewoldt RH, Clasen C, Hosoi AE, McKinley GH (2007) Rheological fingerprinting of gastropod pedal mucus and synthetic complex fluids for biomimicking adhesive locomotion. Soft Matter 3:634−643

Ewoldt RH, Hosoi AE, McKinley GH (2008) New measures for characterizing nonlinear viscoelasticity in large amplitude oscillatory shear. J Rheol 52:1427−1458

Ewoldt RH, Hosoi AE, McKinley GH (2007) Rheological fingerprinting of complex fluids using large amplitude oscillatory shear (LAOS) flow. Ann Trans Nordic Soc Rheol 15:3−8

Fardin MA, Perge C, Casanellas L, Hollis T, Taberlet N, Ortín J, Lerouge S, Manneville S (2014) Flow instabilities in large amplitude oscillatory shear: a cautionary tale. Rheol Acta 53:885−898

Fischer P, Wheeler EK, Fuller GG (2002) Shear-banding structure orientated in the vorticity direction observed for equimolar micellar solution. Rheol Acta 41:35−44

Gallot T, Perge C, Grenard V, Fardin MA, Taberlet N, Manneville S (2013) Ultrafast ultrasonic imaging coupled to rheometry: Principle and illustration. Rev Sci Instrum 84:045107

Ghannam MT, Esmail MN (1998) Rheological properties of aqueous polyacrylamide solutions. J Appl Polym Sci 69:1587−1597

Goudoulas TB, Pan S, Germann N (2017) Nonlinearities and shear banding instability of polyacrylamide solutions under large amplitude oscillatory shear. J Rheol 61:1061−1083

Graessley WW (1980) Polymer chain dimensions and the dependence of viscoelastic properties on concentration, molecular weight and solvent power. Polymer 21:258−262

Hyun K, Wilhelm M, Klein CO, Cho KS, Nam JG, Ahn KH, Lee SJ, Ewoldt RH, McKinley GH (2011) A review of nonlinear oscillatory shear tests: Analysis and application of large amplitude oscillatory shear (LAOS). Prog Polym Sci 36:697−1753

Jaradat S, Harvey M, Waigh TA (2012) Shear-banding in polyacrylamide solutions revealed via optical coherence tomography velocimetry. Soft Matter 8:11677−11686

Kamal MS, Sultan AS, Al-Mubaiyedh UA, Hussein IA (2015) Review on polymer flooding: rheology, adsorption, stability, and field applications of various polymer systems. Polym Rev 55:491−530

Kulicke WM, Porter PS (1980) Relation between steady shear flow and dynamic rheology. Rheol Acta 19:601−605

Kulicke WM, Kull AH, Kull W, Thielking H, Engelhardt J, Pannek JB (1996) Characterization of aqueous carboxymethylcellulose solutions in terms of their molecular structure and its influence on rheological behaviour. Polymer 37:2723−2731

Larson RG, Desai PS (2015) Modeling the rheology of polymer melts and solutions. Annu Rev Fluid

Mech 47:47−65

Lewandowska K (2007) Comparative studies of rheological properties of polyacrylamide and partially hydrolyzed polyacrylamide solutions. J Appl Polym Sci 103:2235−2241

Pan S, Germann N (2020) Mechanical response of industrial benchmark lipsticks under large-scale deformations. Acta Mech 231:3031−3042

Pipkin AC (1986) Lectures on viscoelasticity theory. Springer-Verlag New York

Phan-Thien N, Mai-Duy N (2017) Understanding viscoelasticity. Springer International Publishing

Rao MA (2014) Rheology of fluid and semisolid foods: Principles and applications. Springer US

Reiner M (1964) The deborah number. Phys Today 17:62

Saint-Michel B, Gibaud T, Leocmach M, Manneville S (2016) Local oscillatory rheology from echography. Phys Rev Appl 5:034014

Schramm G (2000) A practical approach to rheology and rheometry. Gebrueder HAAKE GmbH

Shiratori T, Tasaka Y, Murai Y, Takeda Y (2013) Development of ultrasonic visualizer for capturing the characteristics of viscoelastic fluids. J Vis 16:275−286

Shiratori T, Tasaka Y, Murai Y (2016) Rapid rheological characterization of a viscoelastic fluid based on spatiotemporal flow velocimetry. Exp Therm Fluid Sci 71:1−13

Sui C, McKenna GB (2007) Instability of entangled polymers in cone and plate rheometry. Rheol Acta 46:877−888

Takeda Y (1986) Velocity profile measurement by ultrasound Doppler shift method. Int J Heat Fluid Flow 7:313−318

Takeda Y (ed) (2012) Ultrasonic Doppler velocity profiler for fluid flow. Springer Japan

Tasaka Y, Kimura T, Murai Y (2015) Estimating the effective viscosity of bubble suspensions in oscillatory shear flows by means of ultrasonic spinning rheometry. Exp Fluids 56:1−13

Tasaka Y, Yoshida T, Rapberger R, Murai Y (2018) Linear viscoelastic analysis using frequency-domain algorithm on oscillating circular shear flows for bubble suspensions. Rheol Acta 57:229−240

van der Linden E, Sagis L, Venema P (2003) Rheo-optics and food systems. Curr Opin Colloid Interface Sci 8:349−358

Wagner NJ (1998) Rheo-optics. Curr Opin Colloid Interface Sci 3:391−400

Yoshida T, Tasaka Y, Murai Y (2017) Rheological evaluation of complex fluids using ultrasonic spinning rheometry in an open container. J Rheol 61:537−549

Yoshida T, Tasaka Y, Tanaka S, Park HJ, Murai Y (2018) Rheological properties of montmorillonite dispersions in dilute NaCl concentration investigated by ultrasonic spinning rheometry. Appl Clay Sci 161:513−523

Yoshida T, Tasaka Y, Murai Y (2019a) Efficacy assessments in ultrasonic spinning rheometry: Linear viscoelastic analysis on non-Newtonian fluids. J Rheol 63:503−517

Yoshida T, Tasaka Y, Murai Y (2019b) Effective viscoelasticity of non-Newtonian fluids modulated by large-spherical particles aligned under unsteady shear. Phys Fluids 31:103304

Yoshida T, Tasaka Y, Fischer P (2019c) Ultrasonic spinning rheometry test on the rheology of gelled food for making better tasting desserts. Phys Fluids 31:113101